Hybridization-Switching Induced Mott Transition in ABO_3 Perovskites

Atanu Paul,[1] Anamitra Mukherjee,[2] Indra Dasgupta,[1] Arun Paramekanti,[3] and Tanusri Saha-Dasgupta[4,5,*]

[1]*Department of Solid State Physics, Indian Association for the Cultivation of Science, Kolkata 700 032, India*
[2]*School of Physical Sciences, National Institute of Science Education and Research, HBNI, Jatni 752050, India*
[3]*Department of Physics, University of Toronto, Toronto, Ontario, Canada M5S 1A7*
[4]*Department of Condensed Matter Physics and Materials Science, S.N. Bose National Centre for Basic Sciences,
Kolkata 700098, India*
[5]*Center for Mathematical, Computational and Data Science, Indian Association for the Cultivation of Science,
Kolkata 700 032, India*

We propose the concept of a "hybridization-switching induced Mott transition" which is relevant to a broad class of ABO_3 perovskite materials including $BiNiO_3$ and $PbCrO_3$ that feature extended $6s$ orbitals on the A-site cation (Bi or Pb), and a strong A-O covalency induced ligand hole. Using *ab initio* electronic structure and slave rotor theory calculations, we show that such systems exhibit a breathing phonon driven A-site to oxygen hybridization-wave instability which conspires with strong correlations on the B-site transition metal ion (Ni or Cr) to trigger a Mott insulating state. This class of systems is shown to undergo a pressure induced insulator to metal transition accompanied by a colossal volume collapse due to ligand hybridization switching.

Recent advances in transition metal oxides have led to a renewed interest in correlation driven metal-insulator transitions (MITs) [1–9]. Such MITs have been extensively explored in the ABO_3 perovskite family of materials, in which the A-site and B-site cations live on interpenetrating (nominally) cubic lattices. In typical perovskites, the A-site ion is passive, while the B-site transition metal (TM) ion actively dictates the electronic response. The A-site ion controls electronic properties only *indirectly*: its size tunes B-O-B bond angles and thus the B-electron bandwidth, while its charge determines the electron filling. For instance, experimental [10–26] and theoretical [27–37] studies of perovskite nickelates $RNiO_3$ (R being a rare-earth ion) have shown that varying R, with increasing ionic sizes, induces a Mott insulator to metal transition driven by increase in the Ni bandwidth.

In significant contrast to the above scenario, recent experiments on $BiNiO_3$ [38] and $PbCrO_3$ [39], reveal a distinct behavior. $BiNiO_3$, with the large Bi cation at the A site, is an insulator rather than a metal at ambient pressure [40]. This insulator becomes metallic at a critical pressure of 3.5 GPa, with a significant 2.5% volume contraction. Similarly $PbCrO_3$ exhibits an insulator-to-metal transition at 2.5 GPa [39] with a *colossal* 7.8% volume collapse. Similar large volume shrinking insulator-to-metal transitions have been observed upon heating; this technologically important phenomenon was termed "colossal negative thermal expansion" [45,46].

For $BiNiO_3$, attempts to address its MIT using Hartree-Fock theory [47] and dynamical mean-field theory [48] have focused on models involving only Bi and Ni sites. These studies view the insulator as a checkerboard charge ordered crystal $[Bi_{0.5}^{3+}Bi_{0.5}^{5+}][Ni^{2+}]$, assuming that Bi acts as a valence skipping ion with an attractive U Hubbard interaction, while the high pressure metal results from a valence transition into a uniform $[Bi^{3+}][Ni^{3+}]$ configuration. However, photoemission spectroscopy on the metal [49,50] reveals that the nickel valence state is far from being purely Ni^{3+}. At the same time, Bi^{5+} has an energetically deep $6s$ shell [51] which strongly suppresses Bi^{3+}-Bi^{5+} charge disproportionation. These theories neither considered the crucial role of ligand nor that of the lattice in the MIT. These issues are reminiscent of the "charge disproportionation" debate in insulating $RNiO_3$ and B-site bismuthate $BaBiO_3$ [41–44,52,53]. Indeed, rather than being Ni^{2+}-Ni^{3+} charge crystals, the $RNiO_3$ insulators feature a NiO_6 breathing mode instability, leading to site-selective Mott insulators; holes on one Ni sublattice undergo a Mott transition while holes on the other sublattice reside in NiO_6 molecular orbitals [30,31,52,53].

In this Letter, we show that a natural solution to volume collapse MIT in ABO_3 perovskites like $BiNiO_3$ or $PbCrO_3$ emerges if the oxygen sites and lattice distortions are explicitly included in modeling these novel perovskites. In steps towards this, we first show, using density functional theory (DFT) on $BiNiO_3$ and $PbCrO_3$, that the key to their phenomenology lies in an active A site with a $6s$ orbital which can strongly hybridize with oxygen, driving the system to negative charge transfer regime, thereby creating a ligand hole. Based on this, we propose a model for such perovskites which includes all three ions (A, B, O) and the

lattice degree of freedom, and solve it using slave rotor theory. We find that when the oxygen energy level is closer to that of the A-site cation, the system permits an A-O breathing mode instability, which leads to a three-dimensional (3D) checkerboard pattern of compressed and expanded AO_{12} polyhedra. This is analogous to a 3D Peierls' transition in a strongly correlated regime, which does not rely on Fermi surface nesting [54,55]. This instability suppresses the B-O hybridization, triggering a Mott insulating state due to strong correlations on the B-site ions. Applying pressure shifts the ligand energy, favoring B-O hybridization over A-O hybridization. This *hybridization switch* eventually suppresses the A-O breathing mode instability and the concomitant hybridization wave, leading to a metal dominated by B-O states at the Fermi level. Our results motivate us to conclude that $BiNiO_3$ and $PbCrO_3$ belong to a broad category of ligand hole compounds exhibiting *hybridization-switching induced Mott transition.* We propose further material candidates in this category, namely, $TlMnO_3$ and $InMnO_3$.

Pressure-induced structural transition.—At ambient pressure (AP), the crystal structure of $BiNiO_3$ is triclinic, with two inequivalent Bi sites (Bi1, Bi2), and four inequivalent Ni sites. The high pressure (HP) phase, above 3.5 GPa [56], has orthorhombic symmetry, with equivalent Bi and Ni sites. The AP phase has a staggered pattern of compressed and expanded BiO_{12} polyhedra, while the HP phase features BiO_{12} polyhedra of uniform volume. We begin by describing this structural transition within DFT. DFT calculations were carried out in a pseudopotential plane-wave basis with generalized gradient approximation [57] with Hubbard U (GGA + U) [58] ($U = 4$ eV, $J_H = 0.9$ eV), as implemented in the Vienna *ab initio* simulation package [59]; see Supplemental Material (SM) for details [60].

We fit the volume dependence of our DFT cohesive energies of the AP (triclinic) and HP (orthorhombic) structures to the Birch-Murnaghan equation [61]. Using a common tangent construction [see Fig. 1(a)], we find a transition from low-symmetry triclinic to high-symmetry orthorhombic structure with a volume reduction of $\approx 3\%$, in good agreement with high pressure experiments [46].

To understand the role of the bond deformation in the MIT, we computed the stiffness of the Bi-O bonds. Starting from the undistorted orthorhombic structure at volumes corresponding to AP and HP (at 6 GPa), and replacing Ni ions by a uniform positive background, we calculated the energy change δE for small breathing displacement of oxygen atoms (δO) from their equilibrium positions; see Fig. 1(b) inset. Fitting $\delta E = \frac{1}{2} k (\delta O)^2$ yields the Bi-O bond stiffness constants $k_{BiO} = 2.06$ eV/Å^2 and 2.32 eV/Å^2 for AP and 6 GPa HP volumes, respectively. For the Ni-O sublattice, see Fig. 1(b), corresponding calculations yield $k_{NiO} = 7.96$ eV/Å^2 and 10.84 eV/Å^2. Thus, the Ni-O bond, which is stiffer than Bi-O bond, becomes
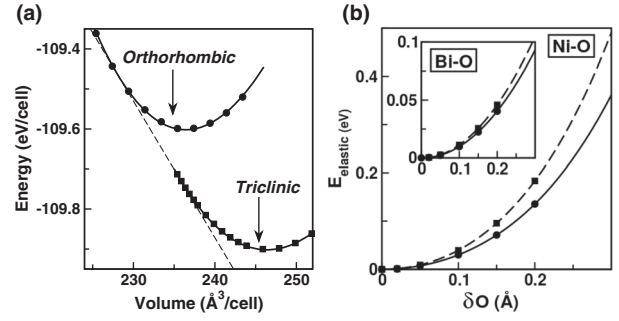

FIG. 1. (a) DFT cohesive energy versus volume for AP (triclinic) and HP (orthorhombic) $BiNiO_3$; the intersection points of the plotted common tangent with the two curves yields the volume change $\Delta V/V \approx 3\%$ at the transition. (b) Elastic energy of the Ni-O sublattice as a function of O-displacement for the HP (dashed) and AP (solid) volumes. Inset shows similar plot for the Bi-O sublattice.

substantially stiffer at HP, suppressing a distortion of the Ni-O sublattice. For comparison, the similarly calculated Ni-O stiffness in $PrNiO_3$, which shows a breathing mode distortion [62], is 7.22 eV/Å^2, a factor of 1.5 smaller than that of HP $BiNiO_3$. This explains the absence of a breathing mode distortion of NiO_6 octahedra in the HP phase, and the resulting stability of the volume-collapsed metal against a Ni "charge-disproportionation" MIT.

DFT electronic structure.—Figure 2(a) shows the spin-polarized GGA + U density of states (DOS) of AP and HP (7 GPa) $BiNiO_3$, respectively, projected onto Bi-s, Ni-d, and O-p states. The Ni-d and O-p plots are the DOS averaged over four inequivalent Ni sites in AP, and six and two O sites in AP and HP, respectively.
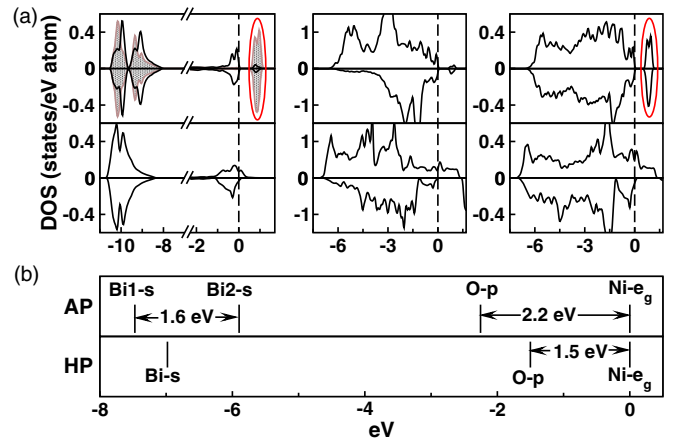

FIG. 2. (a) GGA + U projected DOS of $BiNiO_3$ in AP (top panels) and HP (bottom panels) phase. Left, middle, and right panels show projections to Bi-s (displaying relevant energy ranges), Ni-d, and O-p. Zero of energy is set at GGA + U Fermi energies. For AP, projections to Bi1 (solid, black) and Bi2 (shaded) are shown separately. (b) Calculated energy levels of Bi-s, O-p, and Ni-e_g in the AP and HP phase. Zero of energy is set at Ni-e_g.

At AP, our DFT calculation gives rise to an insulating solution upon including antiferromagnetic (AFM) order. Both Bi1 and Bi2 sites show filled 6s states deep down in energy ≈ 10.5 eV below Fermi level (E_F). The split-off, unoccupied part of Bi2-s states, which is at ≈ 1 eV above E_F, and well separated from the filled Bi2-s states by ≈ 9–10 eV, is entirely derived from strong admixture with O-p states, signaling creation of a ligand hole (see encircled regions in the figure). Thus, the insulator is *weakly* Bi-charge disproportionated [63]. The contribution of Ni-d to this split-off state is small. We find the Ni-d states are filled in the majority spin channel, while in the minority spin channel the octahedral crystal-field split Ni-t_{2g} and Ni-e_g states are, respectively, filled and empty (positioned beyond the energy shown in the figure). This suggests the stabilization of $[\text{Bi1}_{0.5}^{3+}(\text{Bi2}^{3+}\underline{L}^{2(1-\delta)})_{0.5}][\text{Ni}^{2+}\underline{L}^{\delta}]$ configuration in AP, instead of the proposed $[\text{Bi1}_{0.5}^{3+}\text{Bi2}_{0.5}^{3+}][\text{Ni}^{2+}]$ configuration [47,48]. Our calculated oxygen magnetic moment is large ≈ 0.1 μ_B, contrary to the expectation of nonmagnetic O^{2-} for $[\text{Bi1}_{0.5}^{3+}\text{Bi2}_{0.5}^{3+}][\text{Ni}^{2+}]$ configuration. Total energy calculations show that Ni favors a G-type AFM order, in agreement with neutron diffraction [56].

At HP, the DFT calculation gives rise to a metallic solution, with dispersive bands crossing the Fermi level. Our DFT total energy calculations show ferromagnetic Ni-Ni interactions; we therefore predict the HP metal should show ferromagnetic correlations. Analyzing the projected O-p DOS, we again find significant weight at the unoccupied part, reflecting the ligand hole. However, the unoccupied O-p states have a lot more Ni-d character, and much less Bi-s character, compared to the AP phase. Interestingly, the magnetic moment on the Ni site in the HP phase (1.48 μ_B) is not much smaller than in the AP phase (1.73 μ_B), in marked contrast to proposal of Ni^{2+} to Ni^{3+} valence transition between AP and HP. DFT thus suggests stabilization of the $[\text{Bi}^{3+}\underline{L}^{\delta}][\text{Ni}^{2+}\underline{L}^{1-\delta}]$ configuration in the metal. This picture within the single-reference description of DFT is close to the multireference description given by Ni K-edge x-ray absorption spectroscopy [50]. Calculation of crystal orbital Hamiltonian population (COHP) [64,65] (see SM), corroborates the change of ligand hole character from Bi-s to Ni-d.

What causes this shift of oxygen covalency? To answer this, we show in Fig. 2(b), the computed Bi-s, Ni-e_g, and O-p energy level positions in AP and HP phases, obtained from the low-energy tight-binding Hamiltonian in the Wannier function basis within the Nth order muffin-tin-orbital (NMTO) formulation of the downfolding technique [66,67] (see SM). At AP, the s-level energy positions of Bi1 and Bi2, differ by about 1.5 eV, Bi2-s being closer to O-p compared to Bi1-s, leading to stronger covalency between Bi2-s and O-p. Ligand holes are thus preferably associated with Bi2. At HP, the energies of Ni-d and O-p get markedly closer, driving a covalency shift to Ni-O.

Our DFT results for PbCrO$_3$ are qualitatively similar. The quantitative differences in PbCrO$_3$, a smaller critical pressure and larger volume collapse, arise from the O level lying closer to Pb. Thus, the Pb-O covalency is stronger than Bi-O. At the same time, Cr t_{2g} orbitals hybridize less effectively with O than Ni e_g (see SM).

Slave rotor theory.—To go beyond the DFT $+ U$ treatment of the strong correlation effect, and capture the Mott transition without any assumption of magnetic ordering, we next investigate such ABO_3 perovskites in a DFT-inspired "s-p-d" model, which we study using slave rotor mean field theory [68–72]. Our work represents a novel application of slave rotor theory which simultaneously treats all three ions (A, B, O). In contrast to previous work [47,48], our proposed model does not include a phenomenological *negative U* on the A site. Instead, we include phonon distortion and A-O hybridization, which provides a more meaningful microscopic picture [73,74].

Our model for ABO_3 consists of a multiorbital manifold on the B site, with nondegenerate orbitals on A and on the oxygen site. The on-site energies are denoted by ϵ_A, ϵ_B, and ϵ_{Ox}; we fix $\epsilon_B = 0$. Denoting A-O and B-O hopping amplitudes in the symmetric phase as t_A, t_B, respectively, and including a Hubbard $U > 0$ on the B site, yields the Hamiltonian $H = H_1 + H_2 + H_3 + H_4$, with

$$H_1 = \epsilon_A \sum_{\mathbf{r},\sigma} a_{\mathbf{r}+\Delta,\sigma}^{\dagger} a_{\mathbf{r}+\Delta,\sigma} + \epsilon_{Ox} \sum_{\mathbf{r},\sigma,\delta} \ell_{\mathbf{r}+\delta,\sigma}^{\dagger} \ell_{\mathbf{r}+\delta,\sigma}$$

$$H_2 = -t_B \sum_{\mathbf{r}\alpha\sigma\delta} g_{\alpha\delta}(b_{\alpha,\mathbf{r},\sigma}^{\dagger}[\ell_{\mathbf{r}+\delta,\sigma} + \ell_{\mathbf{r}-\delta,\sigma}] + \text{H.c.})$$

$$+ \frac{U}{2} \sum_{\mathbf{r}} \left(\sum_{\alpha\sigma} b_{\alpha,\mathbf{r},\sigma}^{\dagger} b_{\alpha,\mathbf{r},\sigma} - 2 \right)^2$$

$$H_3 = -t_A \sum_{\mathbf{r},\delta,\eta_\delta,\sigma} [1 + \varphi(-1)^{\mathbf{r}}](a_{\mathbf{r}+\Delta,\sigma}^{\dagger} \ell_{\mathbf{r}+\Delta+\eta_\delta,\sigma} + \text{H.c.})$$

$$H_4 = 12N \times \frac{1}{2}\kappa\varphi^2$$

where a, b, ℓ denote electron operators on A, B, and the ligand site, respectively, with α labeling B-site orbitals. Here H_1 describes the on-site energy, with a choice $\epsilon_B = 0$, while H_2 and H_3, respectively, describe the B-O and A-O electronic Hamiltonians, and H_4 denotes the elastic energy cost of A-O bond deformations. Based on DFT, we assume the stiffer B-O sublattice to be immune to breathing distortion. Staggered A-O hopping, $t_A(1 \pm \varphi)$, permits us to capture the A-O *hybridization wave*. In the symmetric phase $\varphi = 0$. In the distorted phase $\varphi = \beta(\delta a_{AO}/a_{AO})$, where $\beta \equiv (\partial \ln t_A / \partial \ln a_{AO})$, and δa_{AO} is the change in A-O bond length compared to its undistorted value a_{AO}. The elastic energy cost in H_4 is $\frac{1}{2}\kappa\varphi^2$ per bond, where $\kappa = ka_{AO}^2/\beta^2$, with spring stiffness constant k, and 12N A-O bonds. For BiNiO$_3$, we have two e_g orbitals ($1 \equiv d_{x^2-y^2}$, $2 \equiv d_{3z^2-r^2}$) at the Ni site, with
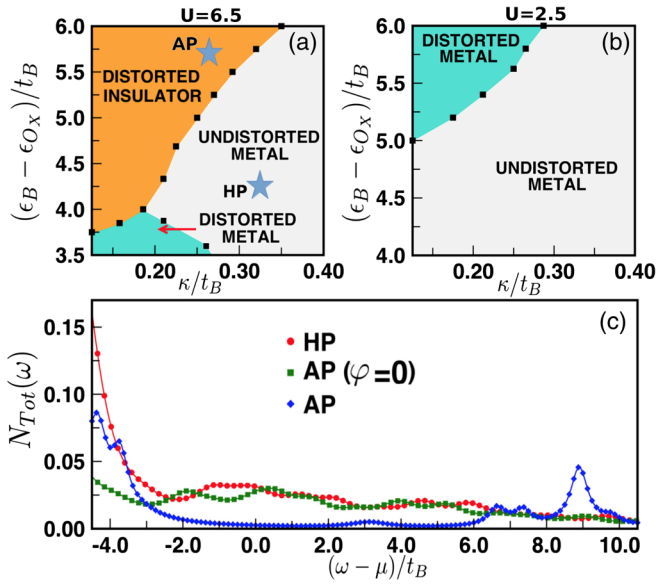
FIG. 3. Phase diagram varying κ and $\epsilon_B - \epsilon_{Ox}$ for (a) $U/t_B = 6.5$ and (b) $U/t_B = 2.5$. (c) DOS $N_{\text{Tot}}(\omega)$ for typical points in AP and HP phases, marked by stars in (a), as well as DOS for the metastable AP phase with imposed $\varphi = 0$.

FIG. 4. Bond-dependent kinetic energy from the model (color bar shows magnitude) for B-O and A-O sublattices in the AP [(a) and (b)] and HP [(d) and (c)] phase, projected to the xy plane. Constant amplitude surfaces of DFT O-p Wannier functions for BiNiO$_3$ at AP (e) and HP (f), superposed on NiO$_6$ octahedra with adjacent two Bi ions. Cyan (light) and magenta (dark) colors indicate opposite signs.

$g_{1,x/y/z} = \{1, -1, 0\}$ and $g_{2,x/y/z} = (1/\sqrt{3})\{-1, -1, 2\}$ due to the orbital-dependent Ni to ligand hopping [75]. This model can be extended to study t_{2g} orbitals relevant to Cr in PbCrO$_3$.

We study the zero temperature phase diagram of Hamiltonian H using slave rotor mean field theory on the B site (see SM for details). This approach ignores fluctuations of the rotor field as well as gauge fluctuations; nevertheless, it reasonably captures strong correlation effects [68–72]. We work in units with $t_B = 1$. We choose $(\epsilon_A - \epsilon_B)/t_B = 8$, $t_A/t_B = 2.5$, and vary κ and ϵ_{Ox}, with $\epsilon_A < \epsilon_{Ox} < \epsilon_B$. Some variation in these parameters does not qualitatively affect our main results. Figure 3 shows the phase diagram with varying ligand energy and stiffness κ, for a B-site ion with (a) $U/t_B = 6.5$, and (b) $U/t_B = 2.5$. For significant κ, when ϵ_{Ox} is close to ϵ_B, the ground state is an undistorted metal (UM) with noninteger B-site occupancy n_B. Tuning ϵ_{Ox} towards ϵ_A, or κ to smaller values, leads to a transition into either a distorted Mott insulator (DI) with pinned $n_B = 2$ (i.e., a "doping tuned" Mott transition on B site), or a distorted metal (DM), depending on U. The strongly correlated case, $U/t_B = 6.5$, which results in a Mott localized DI, mimics the Ni site in BiNiO$_3$; for $t_B = 0.75$ eV, we get $U \approx 5$ eV. Thus, a spontaneous A-O hybridization-wave $\pm\varphi$ cooperates with a large U on the B site, resulting in a *hybridization-switching induced Mott insulator*.

The critical value $(\epsilon_B - \epsilon_{Ox})_{\text{crit}}$ for the MIT increases with increasing κ. At the indicated point in the DI phase in Fig. 3(a), with $\kappa \approx 0.25$, the optimal distortion $\varphi \approx 0.55$. Choosing $\beta \approx 5$ [76] and $a_{\text{BiO}} = 2.3$ Å yields
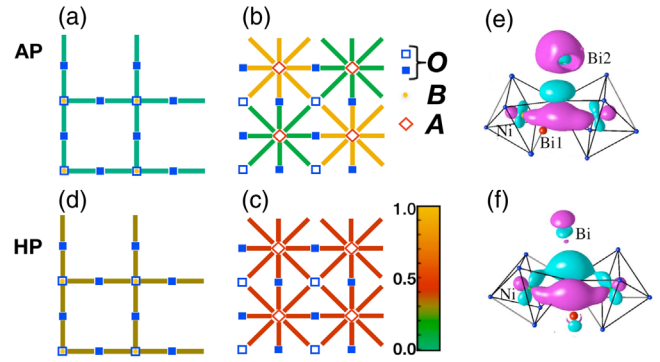
$\delta a_{AO} \approx 0.25$ Å as seen in BiNiO$_3$. Setting $t_B = 0.75$ eV, we get $(\epsilon_B - \epsilon_{Ox})_{\text{crit}} \approx 3.8$ eV for metallization, while the κ value implies a stiffness $k \approx 1$ eV/Å^2, in reasonable agreement with DFT given the simplicity of the model which retains only Ni e_g and a single ligand orbital. The DOS, shown in Fig. 3(c), displays a Mott gap in the DI phase while it is metallic in the UM phase. Forcing $\varphi = 0$ within the DI phase leads to a metallic DOS [see Fig. 3(c)]; correlations alone are thus *insufficient* to induce an insulator.

Bond dependent hybridization.—Figures 4(a)–4(d) show the bond-dependent kinetic energy on the A-O and B-O bonds from the model Hamiltonian. In the DI phase, the B-O hybridization is weak, while AO_{12} polyhedra display the hybridization wave. In the UM phase, on the other hand, the B-O hybridization strengthens significantly compared to that in insulating phase, while the A-O hybridization becomes uniform. We corroborate this using NMTO-downfolding-derived DFT Wannier function plots of BiNiO$_3$ in O-p only basis calculations, as shown in Figs. 4(e) and 4(f) [77]. At AP, the Wannier function is highly asymmetric, having a pronounced tail at Bi2 and nearly vanishing at Bi1. At HP, on the other hand, it is symmetric between Bi sites. Moving from AP to HP the tail at Ni is strengthened significantly, highlighting the change from a Bi s-like to Ni d-like ligand hole.

Conclusion.—We have proposed the concept of a hybridization-switching induced Mott transition in ABO_3 perovskites, with BiNiO$_3$ and PbCrO$_3$ as concrete examples. Using DFT and slave rotor theory, we have identified its key ingredients as follows: (a) extended A-site orbitals which strongly hybridize with oxygen, generating negative charge transfer induced ligand holes and covalent A-O bonds susceptible to breathing distortion (b) strong correlations on the B-site ion. Pressure tuning the oxygen energy

produces a volume-collapse Mott insulator to metal transition via shift in covalency. Based on our study, we propose $TlMnO_3$ [78,79], and even $5s$ systems like $InMnO_3$, as further promising material candidates [80]. Charge doping such Mott insulators may lead to polaronic transport and superconductivity.

[*] t.sahadasgupta@gmail.com

[1] N. F. Quackenbush, J. W. Tashman, J. A. Mundy, S. Sallis, H. Paik, R. Misra, J. A. Moyer, J.-H. Guo, D. A. Fischer, J. C. Woicik, D. A. Muller, D. G. Schlom, and L. F. J. Piper, Nano Lett. **13**, 4857 (2013).

[2] E. Dagotto, Science **309**, 257 (2005).

[3] A. V. Boris, Y. Matiks, E. Benckiser, A. Frano, P. Popovich, V. Hinkov, P. Wochner, M. Castro-Colin, E. Detemple, V. K. Malik, C. Bernhard, T. Prokscha, A. Suter, Z. Salman, E. Morenzoni, G. Cristiani, H.-U. Habermeier, and B. Keimer, Science **332**, 937 (2011).

[4] T.-H. Kim, M. Angst, B. Hu, R. Jin, X.-G. Zhang, J. F. Wendelken, E. W. Plummer, and A.-P. Li, Proc. Natl. Acad. Sci. U.S.A. **107**, 5272 (2010).

[5] C. Giannetti, M. Capone, D. Fausti, M. Fabrizio, F. Parmigiani, and D. Mihailovic, Adv. Phys. **65**, 58 (2016).

[6] M. Imada, A. Fujimori, and Y. Tokura, Rev. Mod. Phys. **70**, 1039 (1998).

[7] J. Zaanen, G. A. Sawatzky, and J. W. Allen, Phys. Rev. Lett. **55**, 418 (1985).

[8] K. Held, G. Keller, V. Eyert, D. Vollhardt, and V. I. Anisimov, Phys. Rev. Lett. **86**, 5345 (2001); N. F. Mott, J. Phys. **42**, 277 (1981); N. F. Mott and L. Friedman, Philos. Mag. **30**, 389 (1974).

[9] Z.-X. Shen and D. S. Dessau, Phys. Rep. **253**, 1 (1995); M. Kozielski, I. Pollini, and G. Spinolo, J. Phys. C **5**, 1253 (1972).

[10] J. B. Torrance, P. Lacorre, A. I. Nazzal, E. J. Ansaldo, and Ch. Niedermayer, Phys. Rev. B **45**, 8209 (1992).

[11] E. Sakai, M. Tamamitsu, K. Yoshimatsu, S. Okamoto, K. Horiba, M. Oshima, and H. Kumigashira, Phys. Rev. B **87**, 075132 (2013).

[12] J. Garcia-Munoz, J. Rodríguez-Carvajal, and P. Lacorre, Europhys. Lett. **20**, 241 (1992).

[13] J. L. Garcia-Munoz, J. Rodriguez-Carvajal, and P. Lacorre, Phys. Rev. B **50**, 978 (1994).

[14] J. Rodriguez-Carvajal, S. Rosenkranz, M. Medarde, P. Lacorre, M. T. Fernandez-Diaz, F. Fauth, and V. Trounov, Phys. Rev. B **57**, 456 (1998).

[15] M. T. Fernandez-Diaz, J. A. Alonso, M. J. Martinez-Lope, M. T. Casais, and J. L. Garcia-Munoz, Phys. Rev. B **64**, 144417 (2001).

[16] D. Meyers, E. J. Moon, M. Kareev, I. C. Tung, B. A. Gray, J. Liu, M. J. Bedzyk, J. W. Freeland, and J. Chakhalian, J. Phys. D **46**, 385303 (2013).

[17] S. Middey, P. Rivero, D. Meyers, M. Kareev, X. Liu, Y. Cao, J. W. Freeland, S. Barraza-Lopez, and J. Chakhalian, Sci. Rep. **4**, 6819 (2014).

[18] S. Catalano et al., APL Mater. **2**, 116110 (2014).

[19] G. Berner et al., Phys. Rev. B **92**, 125130 (2015).

[20] M. H. Upton, Y. Choi, H. Park, J. Liu, D. Meyers, J. Chakhalian, S. Middey, J. W. Kim, and P. J. Ryan, Phys. Rev. Lett. **115**, 036401 (2015).

[21] E. Mikheev, A. J. Hauser, B. Himmetoglu, N. E. Moreno, A. Janotti, C. G. Van de Walle, and S. Stemmer, Sci. Adv. **1**, e1500797 (2015).

[22] V. Bisogni et al., Nat. Commun. **7**, 13017 (2016).

[23] Y. Lu et al., Phys. Rev. B **93**, 165121 (2016).

[24] S. Middey, J. Chakhalian, P. Mahadevan, J. W. Freeland, A. J. Millis, and D. D. Sarma, Annu. Rev. Mater. Res. **46**, 305 (2016).

[25] G. Fabbris, D. Meyers, J. Okamoto, J. Pelliciari, A. S. Disa, Y. Huang, Z. Y. Chen, W. B. Wu, C. T. Chen, S. Ismail-Beigi, C. H. Ahn, F. J. Walker, D. J. Huang, T. Schmitt, and M. P. M. Dean, Phys. Rev. Lett. **117**, 147401 (2016).

[26] J. Ruppen, J. Teyssier, I. Ardizzone, O. E. Peil, S. Catalano, M. Gibert, J. M. Triscone, A. Georges, and D. vanderMarel, Phys. Rev. B **96**, 045120 (2017).

[27] I. I. Mazin, D. I. Khomskii, R. Lengsdorf, J. A. Alonso, W. G. Marshall, R. M. Ibberson, A. Podlesnyak, M. J. Martinez-Lope, and M. M. Abd-Elmeguid, Phys. Rev. Lett. **98**, 176406 (2007).

[28] S. B. Lee, R. Chen, and L. Balents, Phys. Rev. Lett. **106**, 016405 (2011).

[29] S. B. Lee, R. Chen, and L. Balents, Phys. Rev. B **84**, 165119 (2011).

[30] H. Park, A. J. Millis, and C. A. Marianetti, Phys. Rev. Lett. **109**, 156402 (2012).

[31] S. Johnston, A. Mukherjee, I. Elfimov, M. Berciu, and G. A. Sawatzky, Phys. Rev. Lett. **112**, 106404 (2014).

[32] H. Park, A. J. Millis, and C. A. Marianetti, Phys. Rev. B **89**, 245133 (2014).

[33] E. A. Nowadnick, J. P. Ruf, H. Park, P. D. C. King, D. G. Schlom, K. M. Shen, and A. J. Millis, Phys. Rev. B **92**, 245109 (2015).

[34] A. Subedi, O. E. Peil, and A. Georges, Phys. Rev. B **91**, 075128 (2015).

[35] R. J. Green, M. W. Haverkort, and G. A. Sawatzky, Phys. Rev. B **94**, 195127 (2016).

[36] P. Seth, O. E. Peil, L. Pourovskii, M. Betzinger, C. Friedrich, O. Parcollet, S. Biermann, F. Aryasetiawan, and A. Georges, Phys. Rev. B **96**, 205139 (2017).

[37] J. Varignon, M. N. Grisolia, J. Iniguez, A. Barthélémy, and M. Bibes, npj Quantum Mater. **2**, 21 (2017).

[38] S. Ishiwata, M. Azuma, M. Takano, E. Nishibori, M. Takata, M. Sakata, and K. Kato, J. Mater. Chem. **12**, 3733 (2002).

[39] R. Yu et al., J. Am. Chem. Soc. **137**, 12719 (2015).

[40] Note in the case of $BiNiO_3$, the Bi ion occupies the A site, providing an intricate interplay between the active A site and the active strongly correlated B site, namely Ni. This is unlike the case of $BaBiO_3$ (see, e.g., Refs. [41–44]) having structure and phenomenology similar to rare-earth nickelates, in which the Bi ion, occupying the B site, is at the center of the oxygen octahedra.

[41] C. Franchini, A. Sanna, M. Marsman, and G. Kresse, Phys. Rev. B **81**, 085213 (2010).

[42] C. Franchini, G. Kresse, and R. Podloucky, Phys. Rev. Lett. **102**, 256402 (2009).

[43] K. Foyevtsova, A. Khazraie, I. Elfimov, and G. A. Sawatzky, Phys. Rev. B **91**, 121114(R) (2015).

[44] A. Khazraie, K. Foyevtsova, I. Elfimov, and G. A. Sawatzky, Phys. Rev. B **97**, 075103 (2018).

[45] S. Ishiwata, M. Azuma, M. Hanawa, Y. Moritomo, Y. Ohishi, K. Kato, M. Takata, E. Nishibori, M. Sakata, I. Terasaki, and M. Takano, Phys. Rev. B **72**, 045104 (2005).

[46] M. Azuma, W.-t. Chen, H. Seki, M. Czapski, S. Olga, K. Oka, M. Mizumaki, T. Watanuki, N. Ishimatsu, N. Kawamura, S. Ishiwata, M. G. Tucker, Y. Shimakawa, and J. Paul Attfield, Nat. Commun. **2**, 347 (2011).

[47] M. Naka, H. Seo, and Y. Motome, Phys. Rev. Lett. **116**, 056402 (2016).

[48] S. Kojima, J. Nasu, and A. Koga, Phys. Rev. B **94**, 045103 (2016).

[49] P. Kuiper, G. Kruizinga, J. Ghijsen, G. A. Sawatzky, and H. Verweij, Phys. Rev. Lett. **62**, 221 (1989).

[50] M. Mizumaki, N. Ishimatsu, N. Kawamura, M. Azuma, Y. Shimakawa, M. Takano, and T. Uozumi, Phys. Rev. B **80**, 233104 (2009).

[51] I. Hase and T. Yanagisawa, Phys. Rev. B **76**, 174103 (2007).

[52] K. Haule and G. L. Pascut, Sci. Rep. **7**, 10375 (2017).

[53] A. Mercy, J. Bieder, J. Iniguez, and P. Ghosez, Nat. Commun. **8**, 1677 (2017).

[54] Y. Ishige, T. Sudayama, Y. Wakisaka, T. Mizokawa, H. Wadati, G. A. Sawatzky, T. Z. Regier, M. Isobe, and Y. Ueda, Phys. Rev. B **83**, 125112 (2011).

[55] P. A. Bhobe *et al.*, Phys. Rev. X **5**, 041004 (2015).

[56] M. Azuma, S. Carlsson, J. Rodgers, M. G. Tucker, M. Tsujimoto, S. Ishiwata, S. Isoda, Y. Shimakawa, M. Takano, and J. Paul Attfield, J. Am. Chem. Soc. **129**, 14433 (2007).

[57] J. P. Perdew, K. Burke, and M. Ernzerhof, Phys. Rev. Lett. **77**, 3865 (1996).

[58] V. I. Anisimov, I. V. Solovyev, M. A. Korotin, M. T. Czyzyk, and G. A. Sawatzky, Phys. Rev. B **48**, 16929 (1993).

[59] G. Kresse and J. Furthmuller, Phys. Rev. B **54**, 11169 (1996).

[60] See Supplemental Material at http://link.aps.org/supplemental/10.1103/PhysRevLett.122.016404 for detailed information regarding (i) crystal structures, (ii) DFT computations, (iii) results of COHP calculations, and (iv) formalism and results of slave-rotor mean field theory.

[61] F. Birch, Phys. Rev. **71**, 809 (1947).

[62] M. Medarde, C. Dallera, M. Grioni, B. Delley, F. Vernay, J. Mesot, M. Sikora, J. A. Alonso, and M. J. Martinez-Lope, Phys. Rev. B **80**, 245105 (2009).

[63] We find the charge difference between Bi1-s and Bi2-s to be rather small ($< 2\%$) for choice of three different basis sets, LMTO, LAPW, and plane-wave. We contrast this with manganites, where the charge difference at two Mn sites, increases from from the smallest value of 8% for the single layer compound to 39% for the double layer material, and to 22% for the infinite layer compound [D. Okuyama, Y. Tokunaga, R. Kumai, Y. Taguchi, T. Arima, and Y. Tokura Phys. Rev. B **80**, 064402 (2009)].

[64] R. Dronskowski and P. E. Blöchl, J. Phys. Chem. **97**, 8617 (1993).

[65] F. Boucher and R. Rousseau, Inorg. Chem. **37**, 2351 (1998).

[66] O. K. Andersen and T. Saha-Dasgupta, Phys. Rev. B **62**, R16219 (2000).

[67] Only the positions Ni e_g and O p averaged over different inequivalent sites are shown. The fully filled Ni-t_{2g} have not been considered. The small, but finite splitting within e_g levels of Ni, and p levels of oxygen due to distortion, is not shown for simplicity.

[68] S. Florens and A. Georges, Phys. Rev. B **66**, 165111 (2002).

[69] S. Florens and A. Georges, Phys. Rev. B **70**, 035114 (2004).

[70] B. Lau and A. J. Millis, Phys. Rev. Lett. **110**, 126404 (2013).

[71] S. S. Lee and P. A. Lee, Phys. Rev. Lett. **95**, 036403 (2005).

[72] E. Zhao and A. Paramekanti, Phys. Rev. B **76**, 195101 (2007).

[73] C. M. Varma, Phys. Rev. Lett. **61**, 2713 (1988).

[74] W. A. Harrison, Phys. Rev. B **74**, 245128 (2006).

[75] J. C. Slater and G. F. Koster, Phys. Rev. **94**, 1498 (1954).

[76] G. Grosso and C. Piermarocchi, Phys. Rev. B **51**, 16772 (1995).

[77] The Wannier functions are constructed by the NMTO-downfolding calculation, in which only O-p degrees of freedom are kept active in the basis, rest including Ni-d and Bi-s degrees of freedom being downfolded.

[78] W. Yi, Y. Kumagai, N. A. Spaldin, Y. Matsushita, A. Sato, I. A. Presniakov, A. V. Sobolev, Y. S. Glazkova, and A. A. Belik, Inorg. Chem. **53**, 9800 (2014).

[79] Although the valence of Tl was assumed to be nominally 3+, the first-principles calculations reported in Ref. [78] show that the energies of the formally "unoccupied" Tl 6 s states are substantially lower than expected. The situation is thus analogous to $BiNiO_3$, and a hybridization wave would result in a lower symmetry structure with two inequivalent Tl sites, as observed experimentally [78].

[80] This situation is different from $BiFeO_3$ or $PbTiO_3$, so-called "magnetic ferroelectric" compounds, although these compounds also possess an active A site with extended 6s orbital. $BiNiO_3$ and $PbCrO_3$ are negative-charge transfer compounds, leading to creation of a ligand hole in the A-O sublattice, which can participate in the hybridization wave and hybridization-switching instability. In case of $BiFeO_3$ or $PbTiO_3$, on the other hand, A-O hybridization is relatively weak. Thus, the ligand hole formation and the hybridization wave are strongly suppressed. Rather, A-O hybridization in $BiFeO_3$ and $PbTiO_3$ manifests as stereochemical activity of A site. While the general framework of our proposed three-site problem is capable of handling the electronic description of magnetic ferroelectric compounds, it needs to be extended to include appropriate lattice effect, via inclusion of polar phonon modes. This is a topic for future study.